Korean J. of Chem. Eng., **12**(3), 345-351 (1995)

DICHOTOMOUS BEHAVIOR OF POLYMER MELTS IN ISOTHERMAL MELT SPINNING

Sangheon Lee, Byung Min Kim and Jae Chun Hyun†

Department of Chemical Engineering, Korea University, Seoul 136-701, Korea

(Received 17 November 1994 • accepted 14 February 1995)

Abstract—Isothermal melt spinning experiments have been conducted using two polyethylene melts of low density (LDPE) and high density (HDPE) to produce steady state spinline profiles. The data revealed the threadline extensional viscosity exhibiting a contrasting picture : extension thickening behavior for LDPE and extension thinning one for HDPE. A White-Metzner model having a strain rate-dependent relaxation time was then found to be able to simulate this dichotomy in melt spinning fairly well: the fluids whose relaxation times have smaller strain rate-dependence can fit LDPE data with extension thickening extensional viscosity whereas the fluids whose relaxation times have larger strain rate-dependence can fit HDPE data with extension thinning extensional viscosity. This dichotomous nature of viscoelastic fluids is also believed to be able to explain other similar contrasting phenomena exhibited by polymer melts, such as vortex/no vortex in entry flows, cohesive/ductile fracture modes in extension, and more/less stable draw resonance than Newtonian fluids.

Key words: *Isothermal Melt Spinning, Polyethylene Melts, Extensional Viscosity, White-Metzner Model, Relaxation Time*

INTRODUCTION

Many researchers have reported that viscoelastic fluids depending upon their material characteristics exhibit two different behavior patterns in extensional flows. Bagley and Birks [1960] apparently first found that in capillary converging flow low density polyethylene (LDPE) melts developed vortices while high density polyethylene (HDPE) melts did not. Ballenger and White [1971] discovered through a similar experiment LDPE and polystyrene (PS) producing vortices and polypropylene (PP) not. Chen et al. [1972] conducted both melt spinning and weight-dropping experiments using HDPE and LDPE to find that these two materials showed very contrasting behavior in the experiments: in the melt spinning HDPE produced larger extrudate swell and less spinline attenuation than LDPE and revealed difficulty in the initiation of its spinning due to filament breaks, and in the weight-dropping test LDPE was extended uniformly until its break whereas HDPE immediately necked down in the middle of the sample and then broke.

Ide and White [1978] carried out an experiment using an extensional flow apparatus for HDPE, LDPE, PS, PP, and polymethylmethacrylate (PMMA) and found that on being extended HDPE, PP, and PMMA exhibited ductile failure mode with necking while LDPE and PS cohesive failure mode without necking. The extensional viscosities of HDPE, LDPE, and linear low density polyethylene (LLDPE) melts were compared by Kanai and White [1984] to reveal that HDPE showed an extension thinning extensional viscosity (i.e., the extensional viscosity decreasing with the extension strain rate), LDPE extension thickening extensional viscosity, and LLDPE almost constant extensional viscosity. They used this information in explaining the behavior of these polymer melts in tubular film blowing process.

Similar results were also obtained by Minoshima and White [1986] through a systematic study of various polymer melts in their behavior in the three flows of uniaxial extension, ribbon extrusion, and tubular film blowing and they were then analyzed using the earlier rheological model of Ide and White [1977]. White et al. [1987] and Luo and Mitsoulis [1990] explained the reason why in the converging flows LDPE produces vortices and HDPE not, is that the former develops extension thickening extensional viscosity and the latter extension thinning extensional viscosity. Binding [1988] also suggested that this extension thickening extensional viscosity of LDPE plays a role of stress relieving mechanism in the extensional flow.

As explained above, viscoelastic fluids depending upon their material characteristics exhibit contrasting behavior in extensional flows. This kind of information is quite essential in the design, operation and optimization of many polymer processing steps. Research towards the complete understanding of this matter still continues in both experiments and theory. In this article we investigate the behavior of viscoelastic fluids in melt spinning, a typical extensional flow, in terms of extensional viscosity and the spinline velocity profile.

EXPERIMENTAL

The characteristics of the materials used in the isothermal melt spinning experiments are explained in Table 1. The apparatus for the spinning was the Capirograph manufactured by Toyo Seiki and is schematically depicted in Fig. 1. The operating conditions are given in Table 2.

We measured threadline diameters along the spinning distance from the threadline pictures taken from within the isothermal chamber during the steady state runs of the melt spinning, and then using these data along with the threadline tension measurements, we calculated the velocity, strain rate (velocity gradient), stress, and extensional viscosity of the threadline as functions

†To whom all correspondences should be addressed.

Table 1. The characteristics of the polymer melts used in the spinning experiments

Materials	Density (g/cc)	Melt index (g/10 min)	M_n	M_w	M_z	M_w/M_n	Maker
LDPE 303	0.919	6.0	24,000	195,000	756,000	8.1	Hanyang Chemical Corp., Seoul, Korea
HDPE 5200B	0.964	0.35	17,000	260,000	1,718,000	15.5	Honam Petrochemical Corp., Seoul, Korea

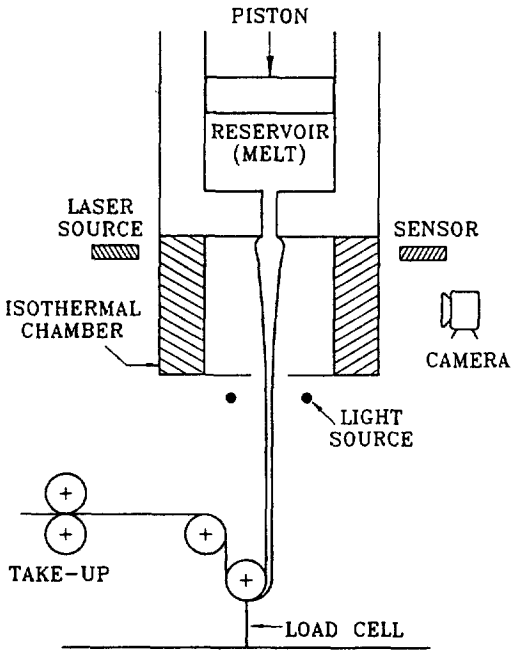

Fig. 1. Schematic diagram of the spinning apparatus.

Table 2. The operating conditions of the spinning experiments

Melt temperature (℃)	180
Capillary die diameter (cm)	0.1 (L/D=10)
Flow rates (cm^3/sec)	0.0119
Spinning length within the isothermal chamber (cm)	10
Spinning length from the spinneret to the take-up (cm)	34
Take-up speed (cm/sec)	8.33, 25.0, 33.3

of the spinning distance from the spinneret.

RESULTS

The experimental data of the threadline diameter, velocity, velocity gradient (strain rate), and stress of the LDPE spinlines plotted against the spinning distance from the spinneret are shown in Figs. 2-5, whereas those of the HDPE spinlines are in Figs. 7-10. They look a lot similar except for the fact that the extrudate swell is pronounced for HDPE cases as shown in Fig. 7 while not so for LDPE cases shown in Fig. 2. However, as displayed in Fig. 6, the extensional viscosity curves of the two cases plotted against the strain rate exhibit the opposite behavior to each other : extension thickening for LDPE and extension thinning for HDPE (The slight extension thickening of HDPE curves at high extension rates is believed due to the possible cooling of the threadlines at the end of the isothermal chamber.). This difference between

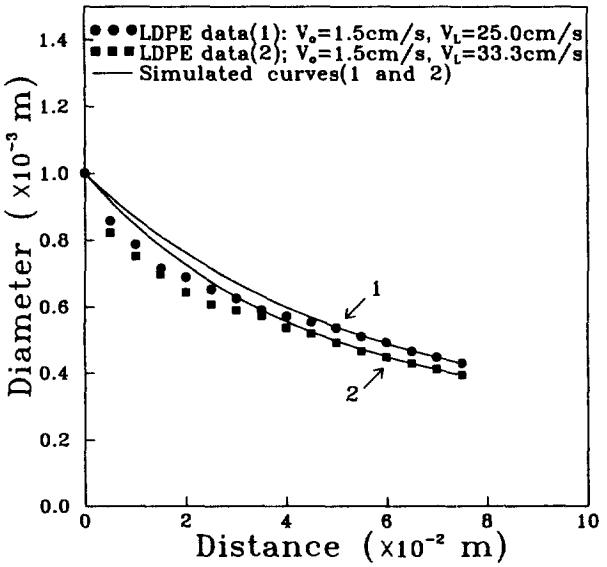

Fig. 2. Experimental and simulated curves of the threadline diameter of LDPE spinlines plotted against the spinning distance.

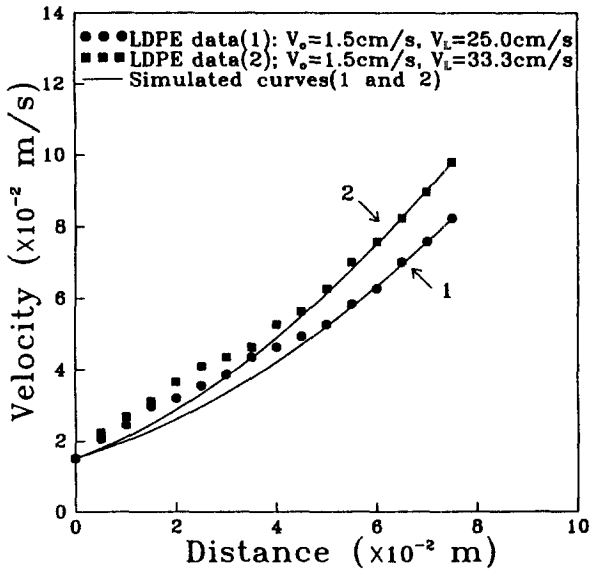

Fig. 3. Experimental and simulated curves of the threadline velocity of LDPE spinlines plotted against the spinning distance.

the two PEs in the extensional deformation data here stands in contrast to the case of shear data where the two PEs produce similar shear thinning behavior as shown in Fig. 11. This kind of opposite behavior of the LDPE and HDPE in the extensional data is not unique to the PEs, but as mentioned in Introduction other polymer melts behave in a similar fashion. The polymer melts in general can thus be dichotomized into two types: exten-

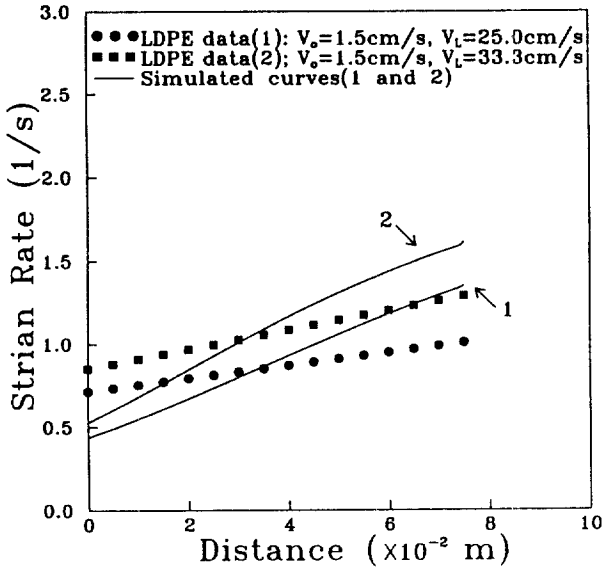

Fig. 4. Experimental and simulated curves of the threadline strain rate of LDPE spinlines plotted against the spinning distance.

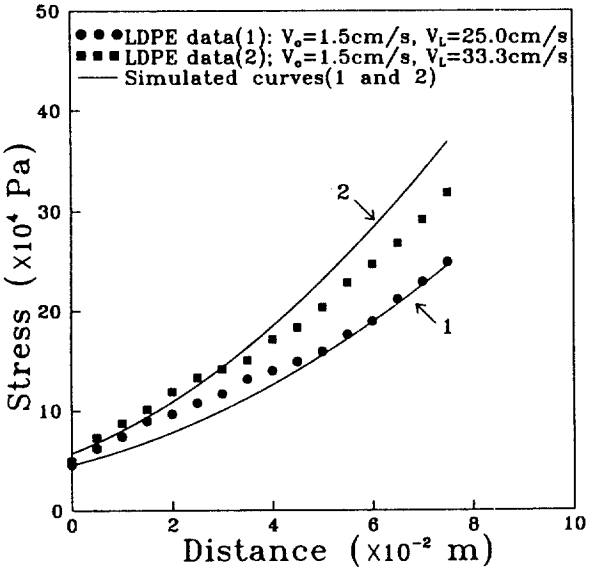

Fig. 5. Experimental and simulated curves of the threadline stress of LDPE spinlines plotted against the spinning distance.

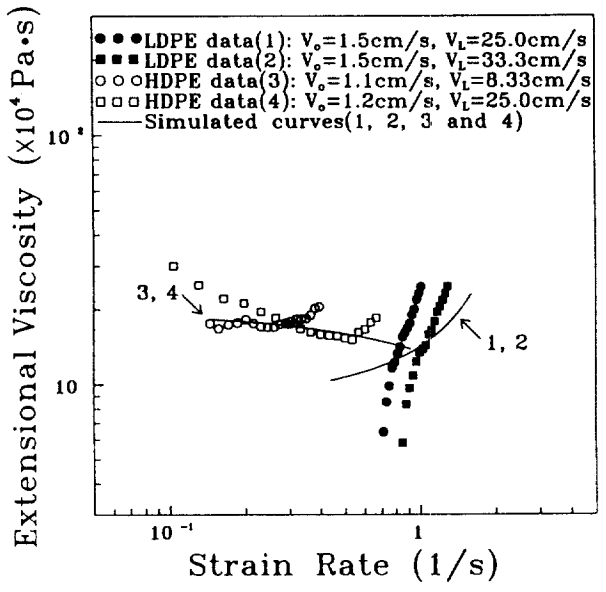

Fig. 6. Experimental and simulated curves of the threadline diameter of HDPE spinlines plotted against the spinning distance.

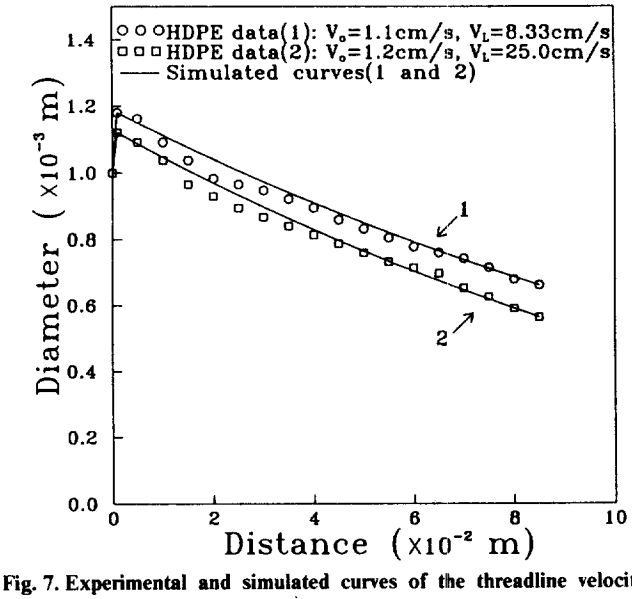

Fig. 7. Experimental and simulated curves of the threadline velocity of HDPE spinlines plotted against the spinning distance.

sion thickening type I fluids like LDPE melts and extension thinning type II fluids like HDPE melts. In the next section we will explain this point using viscoelastic constitutive equations in simulating the melt spinning process.

SIMULATION

The governing equations of isothermal melt spinning are established with the following usual assumptions. (see, for example, Avenas et al. [1975] or Hyun and Ballman [1978].) First, all the secondary forces acting on the threadline, i.e., inertia, gravity, surface tension, and air drag, are neglected to keep the rheological force alone (This assumption is a reasonable one unless the spinning velocity is high and/or the spinning distance is long.). Second, the velocity is uniform across the cross-section of the threadline, and thus we have for the system a one-dimensional model involving the spinning distance coordinate only. Third, the origin of this distance coordinate is chosen where the extrudate swell occurs (This assumption implies that our model does not include the flow history prior to the spinneret nor the subsequent extrudate swell.).

Incorporating the above assumptions and considering the threadline axial stress only, we obtain the following equations for the isothermal melt spinning of a White-Metzner model with a strain rate-dependent relaxation time.

Continuity equation:

$$\left(\frac{\partial A}{\partial t}\right)_x + \left(\frac{\partial (AV)}{\partial x}\right)_t = 0 \tag{1}$$

Equation of motion:

$$\left[\frac{\partial(A\sigma)}{\partial x}\right]_t=0 \tag{2}$$

Constitutive equation:

$$\sigma+\lambda\left[\left(\frac{\partial\sigma}{\partial t}\right)_x+V\left(\frac{\partial\sigma}{\partial x}\right)_t-2\sigma\left(\frac{\partial V}{\partial x}\right)_t\right]=2G\lambda\left(\frac{\partial V}{\partial x}\right)_t \tag{3}$$

Relaxation time:

$$\lambda=\frac{\lambda_0}{1+a\lambda_0\Pi_\Delta} \tag{4}$$

where

A=threadline cross-sectional area
V=threadline velocity
σ=threadline axial stress
x=spinning distance coordinate
t=time
λ=material relaxation time
λ_0=material relaxation time when no strain rate is applied
a=parameter representing the strain rate-dependence of the material relaxation time
Π_Δ=the second invariant of the strain rate tensor=$\sqrt{3}\,\dot{\varepsilon}$ for uniaxial extensional flows
$\dot{\varepsilon}=(\partial V/\partial x)_t$=threadline extensional strain rate=threadline velocity gradient

The above governing equations together with the following boundary conditions are solved to yield the solutions for the threadline.

B.C. 1: at x=0, A=A_0, and V=V_0 (5)

(i.e., the threadline velocity and cross-sectional area at the spinneret are always constant)

B.C. 2: at x=L, V=V_L=rV_0 (6)

(i.e., the threadline velocity at the take-up is maintained constant.) where r=draw-down ratio=V_L/V_0, and the subscripts 0 and L denote the conditions at the spinneret and the take-up, respectively.

Since we in this study seek the steady state solution of the threadline, we set the time derivatives in Eqs. (1) and (3) to zero, which will render threadline throughput and threadline tension force both constant with respect to time and the spinning distance. As derived in the Appendix, this set of governing equations will then yield an analytic solution for the system as shown below.

$$\zeta=\kappa\ \ln\ \xi+\tilde{\lambda}_0\alpha(\xi-1) \tag{7}$$

$$\tilde{\sigma}=\frac{\sigma}{2G}=\frac{\tilde{\lambda}_0}{\kappa}\xi \tag{8}$$

$$\tilde{\dot{\varepsilon}}=\frac{\dot{\varepsilon}L}{V_0}=\frac{\xi}{\kappa+\tilde{\lambda}_0\xi\alpha} \tag{9}$$

$$\tilde{\eta}_E=\frac{\tilde{\sigma}}{\tilde{\dot{\varepsilon}}}=\tilde{\lambda}_0\left[1+\frac{\tilde{\lambda}_0\alpha\xi}{\kappa}\right] \tag{10}$$

$$\alpha=1-a\sqrt{3},\ \tilde{\lambda}_0=\lambda_0\frac{V_0}{L} \tag{11}$$

$$\kappa=\frac{1-\tilde{\lambda}_0\alpha(r-1)}{\ln\ r} \tag{12}$$

Table 3. Comparison of the values of the material functions which best fit the experimental spinning data with those determined from the independent shear rheometer data

Materials \ Expt. data	Spinning data	Shear rheometer data
LDPE	a=0.15	a=0.15
	λ_0=0.53(s)	λ_0=0.44(s)
	G=8.1×10⁴(Pa)	G=8.9×10³(Pa)
HDPE	a=1.2	a=1.2
	λ_0=0.40(s)	λ_0=2.4(s)
	G=2.4×10⁵(Pa)	G=2.2×10⁴(Pa)

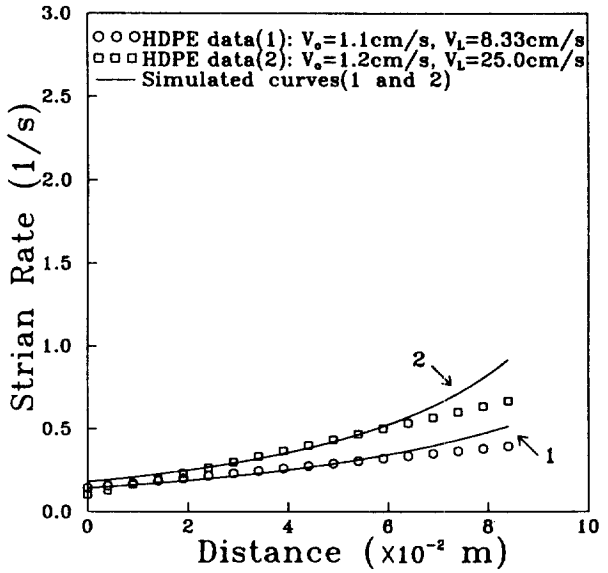

Fig. 8. Experimental and simulated curves of the threadline strain rate of HDPE spinlines plotted against the spinning distance.

where ζ=x/L=dimensionless spinning distance, and ξ=V/V_0=dimensionless threadline velocity.

The profiles of the dimensionless variables of the threadline velocity, stress, strain rate, and extensional viscosity can then be obtained from Eqs. (7), (8), (9), and (10), respectively as the functions of the dimensionless spinning distance, ζ. The profiles of the dimensionless threadline cross-sectional area are also obtained as the reciprocal of the threadline velocity because of $V/V_0=A_0/A$ at steady state.

Now we try to fit the experimental spinning data of LDPE and HDPE by using the above equations with the best values chosen for the material functions of the melts, i.e., 'a', G, and λ_0. We adopted for the parameter 'a' the values obtained from the separately run shear rheometer data shown in Fig. 11, i.e., 'a'=0.15 and 1.2 for LDPE and HDPE, respectively. Then we adjusted the values of G and λ_0 until the simulated curves produced smallest errors (within 0.1 percent) with the corresponding spinning data. The values for G and λ_0 selected this way are shown in the first column of Table 3, which are apparently not in good agreement with those from the shear rheometer data appearing in the second column. The reason for these discrepancies is believed to be the incompleteness of the White-Metzner constitutive equation when simulating different flows of the polymer melts

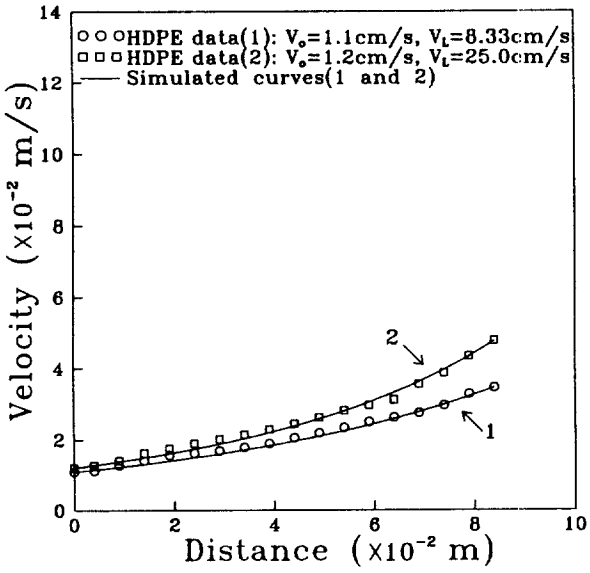

Fig. 9. Experimental and simulated curves of the threadline stress of HDPE spinlines plotted against the spinning distance.

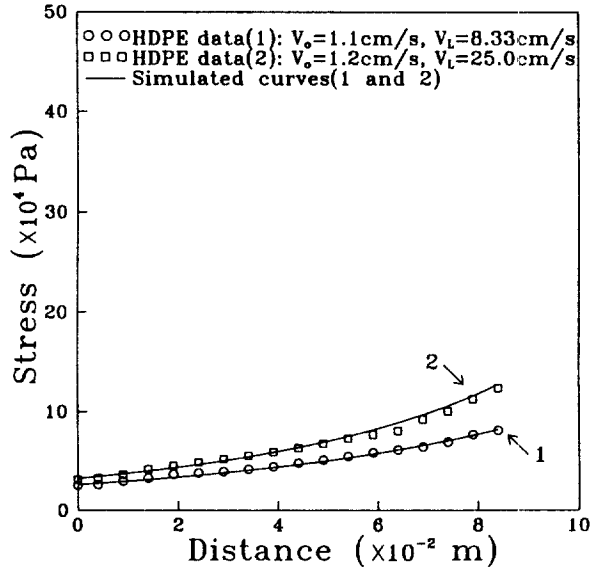

Fig. 10. Experimental and simulated curves of the threadline extensional viscosity of LDPE and HDPE plotted against the strain rate.

with the same material functions. The simulated curves are then displayed as the solid lines in Figs. 2-10. The fitting by these simulated curves to the data is, though, fairly good for all the threadline variables unless the strain rate data are involved, which is due to the fact that the strain rate data represent error-prone slope measurements of the velocity curves.

The important point here is that the White-Metzner model employed with a strain rate-dependent relaxation time is indeed capable of fitting well the isothermal spinning data of LDPE and HDPE (although the adopted values for G and λ_0 are different from those of the shear rheometer data), and, furthermore, of producing qualitatively both extension thickening and thinning behavior of the extensional viscosity. The key is of course the

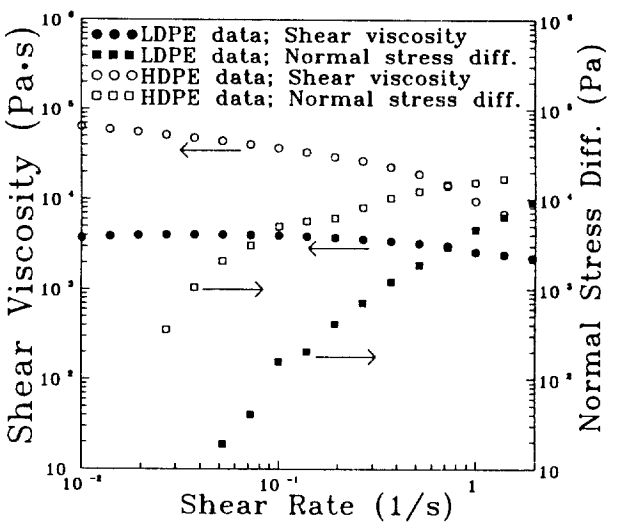

Fig. 11. Shear rheometer data of LDPE and HDPE melts.

parameter, 'a', which represents the extent of the dependence of the material relaxation time on the strain rate as defined by Eq. (4). The value of the parameter 'a' for LDPE turns out to be small, i.e., 0.15 whereas for HDPE large, i.e., 1.2 agreeing with other people's results (e.g., Minoshima and White). In view of the fact that the simple White-Metzner model employed in this study is not expected to produce perfect fit to all spinline profiles, the results in Figs. 2-10 are considered reasonably good and significant.

Next we will show why the White-Metzner model can exhibit both extension thickening and thinning behavior as displayed in Fig. 10 depending on the magnitude of the parameter 'a'.

From Eqs. (9) and (10) we get

$$\tilde{\eta}_E = \tilde{\lambda}_0\left[1+\frac{\tilde{\lambda}_0 a\tilde{\dot{\varepsilon}}}{1-\tilde{\lambda}_0 a\tilde{\dot{\varepsilon}}}\right] \tag{12}$$

from which we can find the sign of $\partial\tilde{\eta}_E/\partial\tilde{\dot{\varepsilon}}$ is the same as that of a. Namely, if $a\gtrless 0$, i.e., $a\lesseqgtr 1/\sqrt{3}$, then $\partial\tilde{\eta}_E/\partial\tilde{\dot{\varepsilon}}\gtrless 0$. Therefore, as shown in Fig. 10, when 'a' is small, the extensional viscosity becomes strain thickening, whereas when 'a' is large, the extensional viscosity does strain thinning.

One additional point deserves mention here. With the White-Metzner model employed in this study, we have the upper limits for both r and $(\lambda_0\,\dot{\varepsilon})$ in isothermal melt spinning as shown below.

Since the reciprocal tension force, K is always positive, from Eq. (A8) we have

$$r_{max} = 1+\frac{1}{\tilde{\lambda}_0 a} \tag{13}$$

Also, since the velocity, V is always positive, from Eq. (A5) we have

$$(\lambda_0\,\dot{\varepsilon})_{max} = \frac{1}{a} \tag{14}$$

Of course, for the type II fluids having negative a values, neither r_{max} nor $(\lambda_0\,\dot{\varepsilon})_{max}$ exist. Of significance is, as shown in Eq. (13), that for the type I fluids having positive a values, the maximum draw-down, r_{max} in isothermal melt spinning is reduced as $\tilde{\lambda}_0 = \lambda_0 V_0/L$ increases. This point is often experienced in actual spinning

experiments.

CONCLUSION

The White-Metzner model having a strain rate-dependent relaxation time can successfully simulate the experimentally observed opposite behavior of the extensional viscosity of LDPE and HDPE melts in isothermal melt spinning. The key to the generation of these dichotomous patterns has turned out to be the parameter representing the extent of the strain rate-dependence of the material relaxation time. This point agrees well with other researchers' findings which show similar contrasting behaviors by the type I and II viscoelastic fluids in extensional flows: vortex/no vortex in entry flows, cohesive/ductile fracture modes in extension, the critical draw ratio for draw resonance being larger/smaller than that of Newtonian fluids, etc.

ACKNOWLEDGMENT

Sincere gratitude is expressed to both Lucky Co., Ltd., Seoul, Korea which provided financial support for this research and to Daelim Industrial Co., Ltd., R & D center, Taejon, Korea which allowed us to use their spinning apparatus.

APPENDIX

The governing equations of isothermal melt spinning expressed by Eqs. (1)-(4) are solved together with the boundary conditions of Eqs. (5) and (6) to yield the solutions for the threadline. Since we are interested in the steady state solution in this study, we set the time derivatives in Eqs. (1) and (3) to zero and then we get the constant flow rate and the constant tension as shown below.

$$AV=Q=\text{constant} \tag{A1}$$

$$A\sigma=F=\text{constant} \tag{A2}$$

where Q=threadline volume flow rate (throughput), and F=threadline tension force.
From these equations, we have

$$\sigma=F/A=(F/Q)\ V \tag{A3}$$

and on substituting this and Eq. (4) into Eq. (3), we obtain

$$V+\frac{dV}{dx}\left[a\sqrt{3}\ \lambda_0 V-\lambda_0\ V-2G\ \lambda_0\left(\frac{Q}{F}\right)\right]=0 \tag{A4}$$

or

$$\frac{dV}{dx}=\frac{V}{\lambda_0(K+V\alpha)} \tag{A5}$$

where $K=2GQ/F$=a reciprocal tension force, and

$$\alpha=1-a\sqrt{3} \tag{A6}$$

Integrating Eq. (A5) from the spinneret ($x=0$, $V=V_0$) to the distance $x(V=V)$, we have

$$x=\lambda_0\ K\ \ln\left(\frac{V}{V_0}\right)+\lambda_0\ \alpha(V-V_0) \tag{A7}$$

The expression for K is easily found by using the boundary condition at the take-up, Eq. (6), as follows.

$$K=\frac{L-\lambda_0\alpha V_0(r-1)}{\lambda_0\ \ln\ r}=\frac{V_0[1-\tilde{\lambda}_0\alpha(r-1)}{\tilde{\lambda}_0\ \ln\ r}=\frac{V_0\kappa}{\tilde{\lambda}_0} \tag{A8}$$

where $\tilde{\lambda}_0=\frac{\lambda_0 V_0}{L}$ = dimensionless relaxation time (A9)

By inserting Eq. (A8) into (A7), we obtain the expression for the threadline velocity as an implicit function of x, which is further rendered dimensionless as shown in Eq. (7).

Next, the threadline stress is calculated as follows. From Eqs. (A3) and (A6), we get

$$\sigma=\frac{2GV}{K} \tag{A10}$$

which on being substituted by Eq. (A8) becomes

$$\sigma=\frac{2G\tilde{\lambda}_0\ \ln\ r}{1-\tilde{\lambda}_0\alpha(r-1)}\ \xi=\frac{2G\tilde{\lambda}_0}{\kappa}\ \xi \tag{A11}$$

The dimensionless threadline stress is then defined as in Eq. (8).

The strain rate, the velocity gradient, is obtained by inserting Eq. (A8) into (A5).

$$\dot{\varepsilon}=\frac{dV}{dx}=\frac{V}{\lambda_0\left(\frac{V_0\kappa}{\tilde{\lambda}_0}+V\alpha\right)} \tag{A12}$$

This is of course the same as the dimensionless expression of Eq. (9).

NOMENCLATURE

- A : threadline cross sectional area
- a : parameter representing the strain rate-dependence of material relaxation times
- F : threadline tension force
- G : material modulus
- K : 2GQ/F
- L : spinning distance between the spinneret and the take-up
- Q : volume flow rate
- r : draw-down ratio
- t : time
- V : threadline velocity
- x : spinning distance coordinate
  $\alpha=1-a\sqrt{3}$
- $\dot{\varepsilon}$: threadline strain rate (velocity gradient)
- $\tilde{\varepsilon}$: dimensionless threadline strain rate
- $\kappa=\frac{1-\tilde{\lambda}_0\alpha(r-1)}{\ln\ r}=\frac{K\lambda_0}{L}$
- λ : material relaxation time
- λ_0 : material relaxation time when no strain rate is applied
- $\tilde{\lambda}_0$: dimensionless material relaxation time=Deborah number $=\lambda_0 V_0/L$
- ζ : dimensionless spinning distance=x/L
- $\tilde{\eta}_E$: dimensionless extensional viscosity=$\tilde{\sigma}/\tilde{\varepsilon}$
- ξ : dimensionless threadline velocity=V/V_0
- σ : threadline axial stress
- $\tilde{\sigma}$: dimensionless threadline axial stress=$\sigma/2G$
- Π_Δ : the second invariant of the strain rate tensor=$\sqrt{3}\ \dot{\varepsilon}$ for uniaxial extensional flows

Subscripts

0 : values at the spinneret
L : values at the take-up

REFERENCES

Avenas, P., Denn, M. M. and Petrie, C. J. S., "Mechanics of Steady Spinning of a Viscoelastic Liquid", *AIChE J.*, **22**, 791 (1975).

Bagley, E. B. and Birks, A. M., "Flow of Polyethylene into a Capillary", *J. Appl. Physics*, **31**, 556 (1960).

Ballenger, T. F. and White, J. L., "The Development of the Velocity Field in Polymer Melts in a Reservoir Approaching a Capillary Die", *J. Appl. Polym., Sci.*, **15**, 1949 (1971).

Binding, D. M., "An Approximate Analysis for Contraction and Converging Flows", *J. Non-Newtonian Fluid Mech.*, **27**, 173 (1988).

Chen, I.-J., Hagler, G. E., Abbott, L. E., Bouge, D. C. and White, J. L., "Interpretation of Tensile and Melt Spinning Experiments on Low Density and High Density Polyethylene", *Trans. of Soc. of Rheol.*, **16**, 473 (1972).

Hyun, J. C. and Ballman, R. L., "Isothermal Melt Spinning-Lagrangian and Eulerian Viewpoints", *J. Rheol.*, **22**, 349 (1978).

Ide, Y. and White, J. L., "Investigation of Failure during Elongational Low of Polymer Melts", *J. Non-Newtonian Fluid Mech.*, **2**, 281 (1977).

Ide, Y. and White, J. L. "Experimental Study of Elongational Flow and Failure of Polymer Melts", *J. Appl. Polym. Sci.*, **22**, 1061 (1978).

Kanai, T. and White, J. L., "Kinematics, Dynamics and Stability of the Tubular Film Extrusion of Various Polyethylenes", *Polym. Eng. Sci.*, **24**, 1185 (1984).

Luo, X.-L. and Mitsoulis, "A Numerical Study of the Effect of Elongational Viscosity on Vortex Growth in Contraction Flows of Polyethylene Melts", *J. Rheol.*, **34**, 309 (1990).

Minoshima, W. and White, J. L., "A Comparative Experimental Study of the Isothermal Shear and Uniaxial Elongational Rheological Properties of Low Density, High Density and Linear Low Density Polyethylenes", *J. Non-Newtonian Fluid Mech.*, **19**, 251 (1986).

Minoshima, W. and White, J. L., "Instability Phenomena in Tubular Film, Melt Spinning of Rheologically Characterized High Density, Low Density and Linear Low Density Polyethylenes", *J. Non-Newtonian Fluid Mech.*, **19**, 275 (1986).

White, S. A., Gotsis, A. D. and Baird, D. G., "Review of the Entry Flow Problem: Experimental and Numerical", *J. Non-Newtonian Fluid Mech.*, **24**, 121 (1987).